Biochimie 243 (2026) 1–15

Contents lists available at ScienceDirect

Biochimie

journal homepage: www.elsevier.com/locate/biochi

Relationship between structure and function of the NADH oxidase from *Lactobacillus brevis*

Mathieu Dondelinger, Marylène S. Vandevenne, Frédéric Kerff, Moreno Galleni *

Centre d'Ingénierie des Protéines, InBios, University of Liege, 13 Allée du 6 Août, B-4000, Liège, Belgium

ARTICLE INFO

Article history:
Received 10 May 2025
Received in revised form
21 December 2025
Accepted 29 December 2025
Available online 17 January 2026

Keywords:
NADH oxidase
Flavoprotein
Lactobacillus brevis
Enzyme dimerisation
Cofactor binding
Protein stability

ABSTRACT

Water-producing NADH oxidases catalyse the oxidation of NADH by molecular oxygen to generate NAD^+ and water. These enzymes require FAD as cofactor to carry out their enzymatic activity and contribute to bacterial protection against oxidative stress. They have received considerable attention since their NAD^+ recycling activity could make them candidates of choice for various industrial oxidoreductive processes. However, most of these enzymes are produced in recombinant hosts (e.g., *E. coli*) as apoenzymes and therefore require activation by incubation with FAD.

In this study, we describe the characterization of the NADH oxidase from *Lactobacillus brevis* (LbNOX), a homodimeric flavoenzyme containing one non-covalently bound FAD molecule per monomer. In this paper, we show that the production, purification and formulation of LbNOX result in a heterogeneous enzyme solution. The active dimeric form is pH dependent and correlates with the presence of FAD. We also performed a comprehensive bioinformatic analysis of the LbNOX structure, which highlights crucial residues for pH-dependent dimerisation and shows that FAD is tightly bound at the dimerisation interface.

This structural and functional characterization is crucial for a complete understanding of the enzyme's activation mechanism and will support the development of a robust and reproducible protocol for the production, purification and formulation of a fully active and homogeneous enzyme solution. More broadly, this work will contribute to the development of NADH oxidases based industrial applications and their FAD-dependent activation mechanism.

1. Introduction

The number of industrial processes and biotransformations that rely on nicotinamide cofactor (NADH or NADP) recycling systems is growing rapidly. One of the most relevant examples of enzymatic reactions coupled to a redox recycling system is alcohol oxidation (Fig. 1), which involves a family of enzymes known as dehydrogenases. These enzymes are widely used to catalyse a broad range of redox reactions in fine chemistry, such as dynamic kinetic resolution of racemic substrates and the synthesis of enantiomerically pure compounds [1]. Since dehydrogenases require nicotinamide cofactors for their catalytic activity, their industrial application must address the challenge of cofactor recycling to achieve efficient and quantitative substrate conversion.

However, despite the growing demand for efficient cofactor recycling systems, significant challenges remain in the development of well-optimized, simple and robust regeneration strategies [2–4]. Cofactor recycling can be achieved through electrochemical or photochemical [5] methods, but the most promising approach relies on enzyme-mediated systems, such as NADH oxidases (NOXs), which use oxygen to oxidize NADH to NAD^+, thereby replenishing the NAD^+ pool [6]. A major limitation of these protein-based systems is that cofactor-dependent oxidoreductases often rely on a stable oligomeric state and tight cofactor binding to maintain their catalytic activity.

NOXs belong to the flavoprotein family. These enzymes catalyse the oxidation of NADH using molecular oxygen, resulting either in water via a complete four-electron reduction, or in hydrogen peroxide (H_2O_2), via a two-electron process [7,8]. Water-producing NOXs are strongly preferred for cofactor regeneration in biotechnological and industrial applications, as they require only oxygen as a substrate and avoid the formation of harmful by-products, producing only NAD^+ and water. In contrast, H_2O_2-producing

* Corresponding author.
E-mail address: mgalleni@uliege.be (M. Galleni).

https://doi.org/10.1016/j.biochi.2025.12.013

Abbreviations

A.U	Absorbance unit
BCA	Bicinchoninic acid assay
BSA	Bovine serum albumin
DSC	differential scanning calorimetry
DSF	differential scanning fluorimetry
IMAC	immobilized metal affinity chromatography
IPTG	isopropyl β-D-1-thiogalactopyranoside
LbNOX	NADH oxydase from *Lactobacillus brevis*
SEC-MALS	size-exclusion chromatography coupled to multi-angle light scattering
Tm	melting temperature

NOXs generate reactive oxygen species or their precursors, which pose significant safety concerns in industrial settings.

Water-forming NOXs have been successfully used for cofactor regeneration in various processes, including the oxidation of 2-heptanol to 2-heptanone [9] and the conversion of glycerol to 1,3-dihydroxyacetone [10]. In this study, we analyse the enzymatic and structural properties, as well as the stability, of the water-forming NOX from *Lactobacillus brevis* (LbNOX, UniProt ID: Q8KRG4). This enzyme is a typical NADH oxidase, structured as a homodimer composed of two 49 kDa subunits, each containing one flavin adenine dinucleotide (FAD) molecule [11].

The catalytic mechanism of water-forming NOXs requires both the active-site residue Cys42 and the FAD cofactor, which are essential for mediating the electron transfers through successive intermediate reactions [12]. A catalytic model proposed by Argyrou & Blanchard (Fig. 2) illustrates these reactions [13].

However, the catalytic mechanism of LbNOX remains incompletely understood. An asymmetric or cooperative model of the two active sites within the homodimer has been suggested, implying that the dimeric form is required for full activity and may enable the inter-monomer electron transfer [14]. The available crystal structure of LbNOX (PDB ID: 5VN0) confirms the homodimeric arrangement and FAD binding, although, as is generally the case in crystallography, transient catalytic intermediates are not resolved. Also, it should be noted that the inter-monomer electron transfer is not reflected in the catalytic model proposed by Argyrou & Blanchard and that the overall stoichiometry of the model is not balanced.

Expressing enzymes, and more generally proteins, with high yield and in a stable, homogeneous and fully active state is a major concern in biotechnology, as it directly impacts the feasibility of using these biocatalysts in large-scale production and robust industrial biotransformations. The greater the stability and activity of the enzyme, the higher its potential for industrial application. Protein stability reflects its ability to maintain a properly folded, native conformation, and is typically assessed by determining its melting temperature (Tm) through thermal denaturation experiments. Beyond this structural definition, an enzyme must also retain its biological activity under various environmental conditions, such as different pH values, buffer compositions, or the presence of excipients and other additives in formulation and reaction buffers.

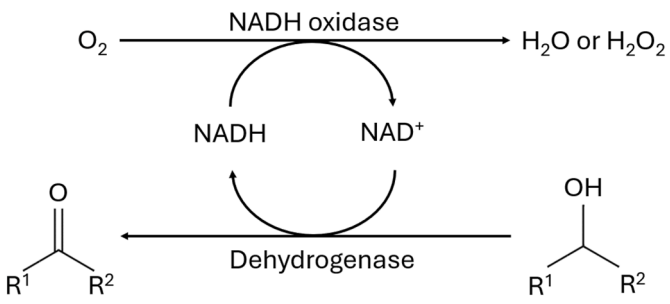

Fig. 1. Enzymatic oxidation of alcohols using a cofactor regeneration system.

This manuscript describes the recombinant expression of LbNOX in *Escherichia coli*. The protein was expressed and purified using immobilized metal affinity chromatography (IMAC) yielding a high amount of pure protein (300 mg per litre of bacterial culture). However, the recombinant LbNOX was found to consist of a mixture of the monomeric apoform (lacking FAD) and the dimeric complex $(LbNOX:FAD)_2$, which exhibits full enzymatic activity. We therefore investigated how the monomeric apoenzyme can be activated by the addition of exogenous FAD to obtain a homogenous solution of fully active protein. In addition, we analysed how both the presence of FAD and the pH influence the equilibrium between the monomeric and dimeric (active) forms of the enzyme. A structure-based interpretation of the results provides hypotheses regarding the molecular mechanism underlying the structure-function relationship of LbNOX and the improvement of its kinetic stability to enhance its biotechnological value.

2. Material and methods

2.1. Production and purification of LbNOX

The gene encoding LbNOX (Uniprot ID Q8KRG4) was synthesized by GeneCust (France), with codon usage optimized for expression in *Escherichia coli*. The gene was cloned into the pET28a plasmid between the *NdeI* and *XhoI* restriction sites and fused at the N-terminal extremity to a His_6-tag using the following linker sequence: MGSSHHHHHHSSGLVPRGS. The integrity of the resulting plasmid was verified by DNA sequencing.

E. coli BL21(DE3) cells were transformed with the resulting plasmid for recombinant protein production. Transformed cells were grown overnight at 37 °C on LB-agar plates containing kanamycin (50 mg L^{-1}) for plasmid selection. A single colony was used to inoculate 5 mL of LB medium containing kanamycin (50 mg L^{-1}), which was incubated for 3 h at 37 °C. This preculture was then used to inoculate 0.5 L of Terrific Broth medium with the same antibiotic concentration. Cultures were grown at 37 °C until the optical density at 600 nm (OD_{600}) reached 1.0–1.4. Protein expression was induced by adding isopropyl β-D-1-thiogalactopyranoside (IPTG) to a final concentration of 300 μM, and cultures were incubated overnight at 18 °C.

Cells were harvested by centrifugation at 3000 g for 30 min at 4 °C. The resulting cell pellet was suspended in 20 mL of lysis buffer (20 mM sodium phosphate, 300 mM NaCl, 20 mM imidazole, pH 7) and disrupted using a French press. The crude lysate was clarified by centrifugation at 14,000 g for 30 min at 4 °C. The resulting supernatant was filtered through a 0.45 μm syringe filter (Merck Millipore).

LbNOX was purified by Ni^{2+}-based immobilized metal affinity chromatography (IMAC), using a HisTrap HP column (Amersham Biosciences) pre-equilibrated with lysis buffer. Chromatography was performed on an NGC Quest™ 100 purification system (Bio-rad). The column was washed with 10 column volumes of lysis buffer, and bound protein was eluted with a linear gradient of 20 column volumes from 0 % to 100 % elution buffer (20 mM sodium phosphate, 300 mM NaCl, 500 mM imidazole, pH 7). Fractions showing a yellow coloration (indicative of FAD content) were pooled together and dialysed 3 h at 4 °C with 12–14 kDa molecular weight cut-off dialysis membrane (Spectrapor®) against formulation buffer (50 mM sodium acetate 150 mM NaCl buffer pH 6). The purified protein was subsequently filtered through 0.22 μm

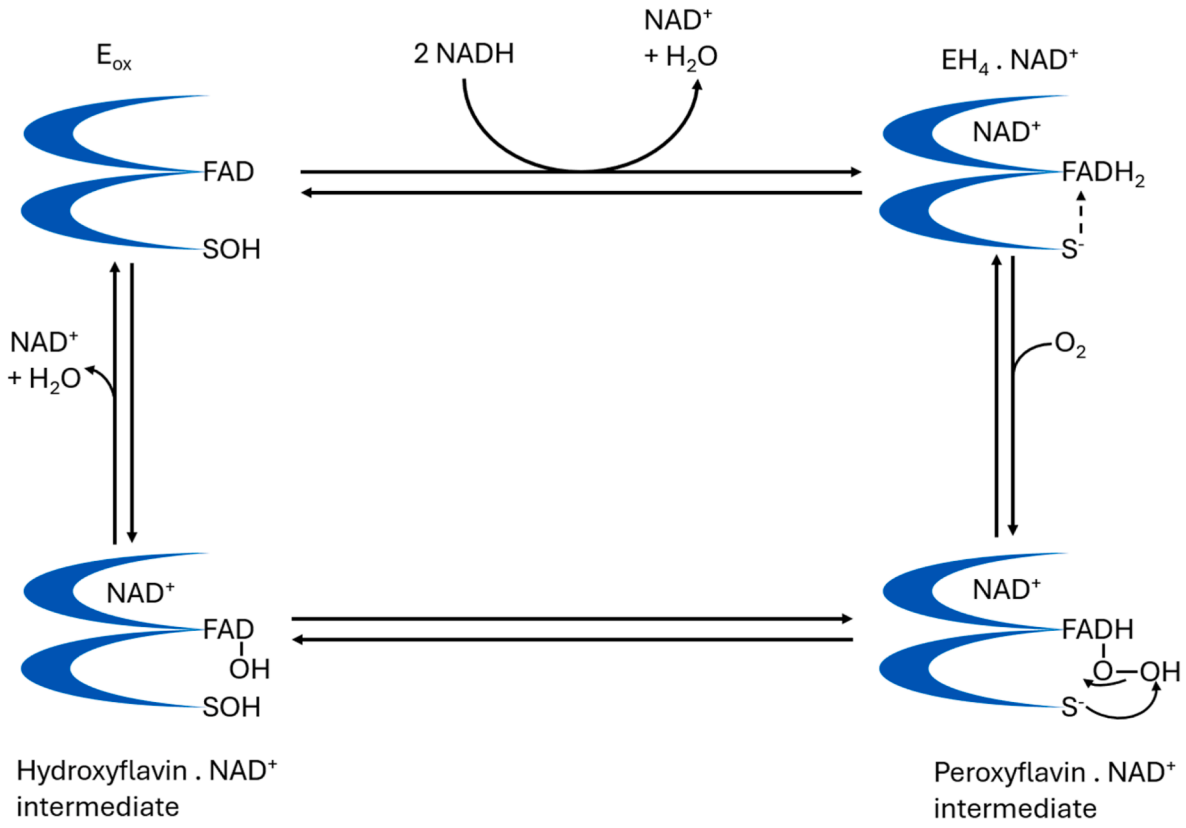

Fig. 2. Proposed catalytic model from Argyrou & Blanchard [13].

filter syringe.

Both the crude lysate and the purified fraction were analysed by SDS-PAGE.

2.2. Determination of LbNOX concentration and its FAD content

A UV–visible spectrum of the purified protein diluted 10 times the in formulation buffer was recorded to determine its concentration (ε_{280} = 36,330 M^{-1} cm^{-1}) and to verify the absence of aggregation. Protein concentration was also assessed using the bicinchoninic acid assay (Pierce™ BCA Protein Assay Kit). To measure the FAD content of LbNOX, 200 μL of enzyme solution was thermally denatured at 90 °C for 1 h. After centrifugation at 16,000 g for 20 min, the supernatant was analysed by UV–visible spectroscopy in the 250–500 nm range. For spectral comparison, both the native LbNOX sample and the denatured supernatant were diluted 10-fold prior to measurement.

FAD concentration was determined from the absorbance at 450 nm (ε_{450} = 11,300 M^{-1} cm^{-1}). Its contribution to the absorbance at 280 nm was subtracted from the overall LbNOX spectrum to estimate the actual protein concentration.

A reference UV–visible spectrum of pure FAD was recorded from a stock solution prepared at 25 μM. The actual concentration was verified spectrophotometrically using ε_{450} = 11,300 M^{-1} cm^{-1}, yielding a corrected concentration of 21 μM. For comparison with LbNOX-bound FAD, the spectrum was scaled to the equivalent of a 2.1 μM solution.

2.3. Size exclusion chromatography

Size exclusion chromatography experiments (SEC) were performed with a Superdex® 200 Increase 10/300 GL column (GE Healthcare) on an NGC Quest™ 100 purification system (Biorad). The column was equilibrated with the appropriate buffer before injection. The purified LbNOX solution was dialysed against buffers of varying pH: 50 mM acetate (pH 6), 50 mM sodium phosphate (pH 7), and 50 mM Tris (pH 8 and pH 9), each supplemented with 150 mM NaCl. For each run, 500 μL of LbNOX (4 mg mL^{-1}) was loaded onto the column at a flow rate of 0.5 mL min^{-1} for 1.5 column volumes.

The column was calibrated using 0.5 mg mL^{-1} bovine serum albumin (BSA, Thermo Scientific) and 0.5 mg mL^{-1} soybean trypsin inhibitor (Sigma) as standards. Fractions of 0.5 mL corresponding to peaks detected at 280 nm were collected and analysed for absorbance spectra and LbNOX activity.

Buffers were prepared at 50 mM concentration with 150 mM NaCl and included: Tris pH 9, Tris pH 8, sodium phosphate pH 7, sodium acetate pH 6, and sodium acetate pH 5. For each collected fraction, a single absorbance spectrum from 250 to 500 nm was recorded using TECAN spectrophotometer (path length = 1 cm), and protein concentration was calculated from the absorbance at 280 nm. Enzymatic activity was measured by adding 1 μL of each fraction to 300 μL of reaction mixture containing 500 μM NADH, 150 mM NaCl, 50 mM phosphate buffer pH 7, with or without 25 μM FAD. Absorbance at 339 nm was monitored for 5 min (path length = 1 cm).

SEC coupled with multi angles light scattering (SEC-MALS) experiments were carried out using a Prominence inert LC system (Shimadzu) coupled with a miniDAWN TREOS II MALS detector (Wyatt technology) and a Superdex® 200 Increase10/300 GL column (GE Healthcare). After equilibration with buffer, 50 μL of LbNOX (1 mg mL^{-1}) was injected and eluted at a flow rate of 0.7 mL min^{-1} over 40 min. The column was calibrated with 1 mg mL^{-1} BSA (Thermo Scientific), as a molecular weight

standard. Peaks were integrated manually. The molecular weight and polydispersity index (Mw/Mn) of each eluted species were determined using ASTRA software (version 7.3, Wyatt Technology). The polydispersity index reflects the width of the molecular weight distribution for each peak: values between 1.000 and 1.050 are considered highly monodisperse samples.

2.4. Purification of the apoenzyme

LbNOX was subjected to SEC on Superdex® 200 Increase 10/300 GL column using Tris buffer at pH 9 to isolate the monomeric, FAD-free form. Two runs were performed, each with 500 μL of protein solution at a concentration of 8.5 mg mL^{-1}. During these first SEC runs, the elution peaks displayed noticeable shoulders, indicating some sample heterogeneity. The fractions from both runs were pooled and concentrated twofold using an Amicon® ultrafiltration membrane (10 kDa molecular weight cut-off). The resulting solution was subjected to a second SEC run. On this chromatogram, the elution peak no longer displayed a shoulder, indicating improved sample homogeneity and suggesting the presence of a single, monodisperse species. In parallel, a UV–visible absorbance spectrum from 250 to 500 nm was recorded on the final fraction to calculate the protein concentration and confirm the absence of significant flavin contamination.

The final purified fraction (~500 μL) had a concentration of 12.9 mg mL^{-1}, corresponding to a recovery yield of approximately 76 %. The sample was aliquoted and stored at −20 °C until further use.

2.5. Activity measurement

For the determination of the optimal pH, LbNOX activity assays were carried out in triplicate using 50 mM buffer supplemented with 150 mM NaCl, 300 μM NADH and 10 μg mL^{-1} BSA. The different buffers used to cover the pH range are listed in Table 1.

Each reaction was carried out in a final volume of 1 mL containing 2 μg of LbNOX. NADH absorbance at 339 nm was monitored for 1 min at 30 °C using a SPECORD® 50 Plus spectrophotometer (Analytik Jena).

To determine the affinity constant of LbNOX for its FAD cofactor, activity assays were performed in 50 mM phosphate buffer supplemented with 150 mM NaCl, 500 μM NADH, 10 μg mL^{-1} BSA and different FAD concentrations ranging from 0 to 5 μM. Reactions were carried out in triplicate in a final volume of 300 μL containing 0.5 μg of LbNOX. NADH absorbance at 339 nm was monitored for 10 min at 20 °C (room temperature) using an Infinite® M200 PRO microplate spectrophotometer (TECAN). Negative controls (no enzyme added) were included for each FAD concentration tested. Slopes for each condition were determined by linear regression within the initial, linear phase of the reaction, and used to calculate specific activity values. Catalytic parameters were then derived from Hanes–Woolf plots constructed from the averaged triplicate data.

For the determination of the catalytic parameters, activity assays were carried out in triplicate in 300 μL of buffer composed of 50 mM sodium phosphate buffer (pH 7.0), 150 mM NaCl, different concentrations of NADH (200, 150, 100, 75, 50, 37.5, 25, 18.75, 12.5 μM) and 10 μg mL^{-1} BSA. Three experimental conditions were tested:

- 0.5 μg mL^{-1} (10 nM) LbNOX without added FAD
- 0.2 μg mL^{-1} (4 nM) LbNOX with 2.5 μM FAD added to the reaction mixture.
- 0.2 μg mL^{-1} (4 nM) pre-activated LbNOX in the absence of FAD in the reaction mixture. Activation was achieved by incubating the enzyme (2 μM) with 5 μM FAD for 1 h on ice.

The absorbance of NADH at 339 nm was monitored for 1 min at 30 °C using a SPECORD® 50 Plus spectrophotometer (Analytik Jena). Catalytic parameters were calculated based on the linear regression of Hanes-Woolf plots generated from the averaged triplicate measurements. Statistical analysis was performed using Microsoft Excel to determine the 95 % confidence intervals for the slope and Y-intercept of the linear regression model. These intervals were then used to estimate the corresponding uncertainty ranges of the catalytic parameters.

Table 1
pH and buffer composition for activity measurement.

pH 5	pH 6	pH 7	pH 8	pH 9	pH10
Na Acetate	Na Acetate Na Phosphate	Na Phosphate Tris	Na Phosphate Tris Glycine	Tris Glycine	Glycine

2.6. Formulation experiment

The formulation experiment was conducted at the Robotein® facility following the protocol described by Kellner et al. [15]. A total of 13 different buffer components were selected to cover a pH range from 2 to 10. Based on these, two sets of buffers were prepared: i) a set of single component buffers at 50 mM; (ii) a set of two-component buffers at 25 mM each. This resulted in 19 chemically distinct buffer mother solutions. Each buffer was then adjusted across its effective buffering range between pH 2.5 and 9.5 in 0.5-unit increments, yielding a total of 158 unique buffer conditions. Fig. 3 provides a schematic overview of the formulation screen, summarising all tested buffer compositions, component combinations, and corresponding pH conditions.

Differential Scanning Fluorimetry (DSF) was used to evaluate protein stability. Samples (0.1 mg mL^{-1} purified LbNOX, *i.e.* 2 μM) were mixed with SYPRO® Orange (Invitrogen Inc., 1:1000 dilution of commercial stock, corresponding to 5X) in a total reaction volume of 40 μL. Measurements were performed using a real-time quantitative PCR machine (Biorad MJ Mini Thermal Cycler equipped with Mini Opticon real-time PCR System). After equilibration of the samples for 5 min at 20 °C, a temperature gradient from 20 to 95 °C was applied. Fluorescence was monitored using the following parameters: $\lambda_{exc.}$ = 470–500 nm, $\lambda_{em.}$ = 540–700 nm.

Apparent melting temperatures (T_m) were determined as the inflexion points of the melting curves, corresponding to the maximum of the first derivative of fluorescence intensity. Data analysis was performed using Wolfram Mathematica software. All screening and analyses were carried out in a fully automated manner at the Robotein® facility.

2.7. Bioinformatics

The structure of LbNOX (PDB ID: 5VN0) was analysed using the PISA software [16] to identify intermolecular interfaces (monomer-monomer and FAD-monomer) as well as the interacting residues.

Structural visualisation and analysis were performed using PyMOL software [17]. Monomeric and dimeric forms of LbNOX were extracted with or without the FAD cofactor and dioxygen. These structural models, as well as the entire crystal structure, were then processed with the PDB2PQR-APBS software [18] to simulate the pH effect on the pKa values of LbNOX residues and thereby investigate their protonation states. Simulations were

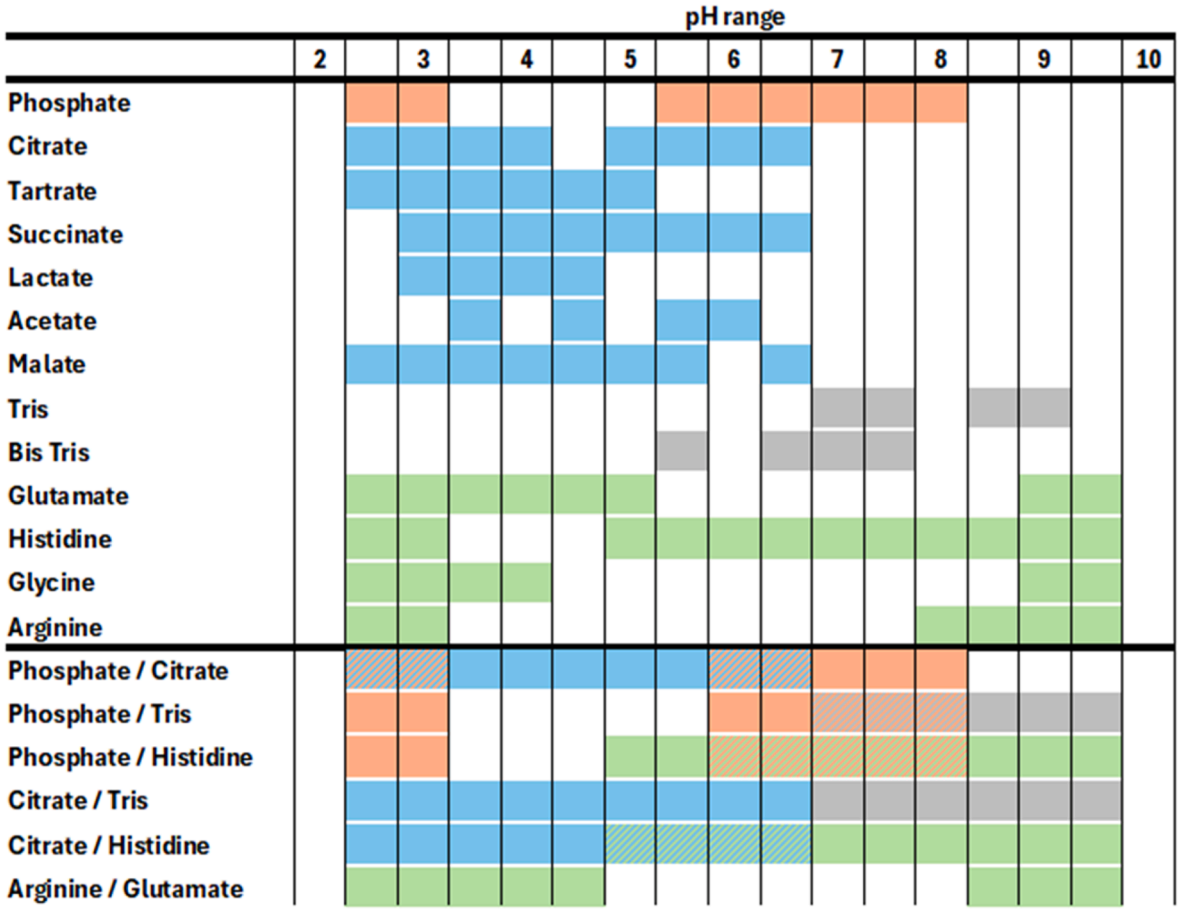

Fig. 3. Overview of all buffer and pH conditions tested in the formulation screen. The buffers were prepared either as single components at 50 mM or as two-component mixtures containing 25 mM of each component. Colours indicate the chemical nature of the buffer component(s): phosphate (orange), carboxylic acids (blue), amines (grey), and amino acids (green). Each square representing one unique formulation condition.

performed across a pH range from 5 to 9, using three force fields: AMBER, CHARMM, and PARSE.

BLASTp [19] analysis using the LbNOX sequence was realised. The analyse was performed against the "non-redundant protein sequences (nr)" database, excluding *Lactobacillus brevis* (Taxid 1580), as well as models and uncultured/environmental sample sequences. Multiple sequence alignment was then performed using Clustal Omega [20].

3. Results

3.1. Production, purification of LbNOX

A synthetic gene encoding the LbNOX protein with an N-terminal His_6-tag was expressed in *E. coli* BL21(DE3). After purification by IMAC, SDS-PAGE analysis confirmed the high purity of the protein, showing a single band at the expected molecular weight (~ 50 kDa; theoretical MW = 51.1 kDa, Supplemental Fig. 1). The protein was stored in sodium acetate buffer (pH 6.0) at −20 °C for subsequent used in enzymatic assays. Based on UV absorbance at 280 nm and BCA assay, the production yield was estimated to be at approximately 600 mg of purified LbNOX per litre of culture.

3.2. Absorbance spectra of purified LbNOX and quantification of FAD content

To assess the presence of FAD in the purified LbNOX solution and estimate the proportion of apo versus holoenzyme, UV absorbance spectra were recorded. FAD exhibits three characteristic absorbance peaks around 260 nm, 360 nm, and 450 nm [21–23], whereas proteins typically show a single maximum around 280 nm due to aromatic residues.

To distinguish protein and cofactor contributions, the LbNOX solution was heat-denatured at 90 °C for 1 h to precipitate the protein. After centrifugation, the supernatant was analysed by UV spectroscopy.

As shown in Fig. 4, the native protein solution displayed a dominant peak at ~280 nm and additional maxima at ~360 nm and ~450 nm, indicating the presence of FAD. After protein precipitation, the spectrum of the supernatant retains characteristic FAD peaks, confirming its presence in the original sample.

Based on the absorbance at 450 nm, the FAD concentration was estimated at 28.4 μM. After correcting for FAD contribution at 280 nm, the protein concentration was determined to be 162 μM, resulting in a FAD/protein ratio of ~17.5 %. This indicates that only a fraction of the purified enzyme carries the FAD cofactor, and the preparation consists mainly of the apoform.

3.3. Quaternary structure analysis of LbNOX and impact of pH

Given the heterogeneity of the LbNOX protein solution revealed by FAD content measurements, we investigated its oligomeric state using size-exclusion chromatography (SEC).

The SEC chromatograms (Fig. 5) show the coexistence of several LbNOX species in solution: (i) a form eluted just after BSA with a retention volume around 14 mL likely corresponding to the

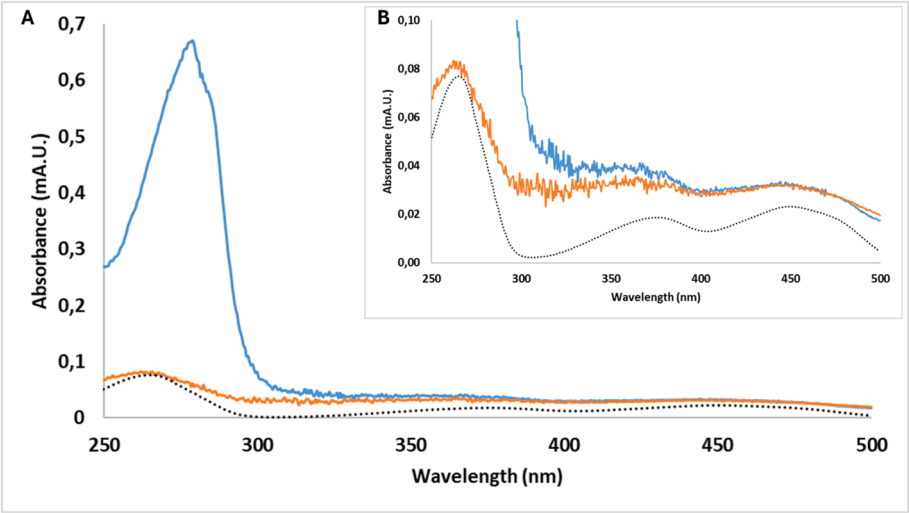

Fig. 4. A. UV–visible spectra of purified LbNOX diluted 10 × (blue), soluble FAD recovered after thermal denaturation (orange) and pure FAD solution at 2.1 μM (dotted black). **B.** Zoom on the 0.00–0.10 A U. range, showing overlapping peaks at 450 nm, confirming FAD presence in the native LbNOX solution.

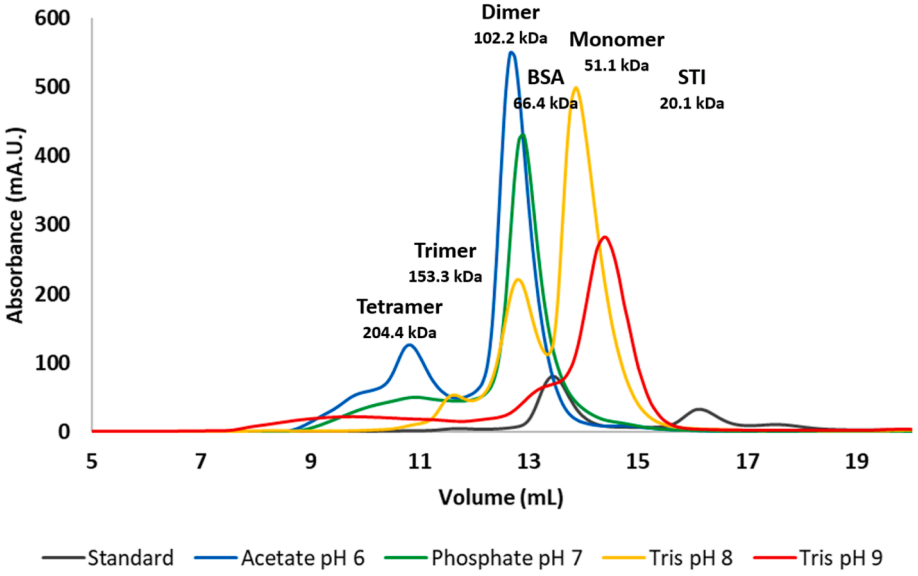

Fig. 5. Size-exclusion chromatograms of LbNOX in different buffer conditions. All buffers contained 50 mM buffer (acetate, phosphate or Tris) and 150 mM NaCl. Blue: acetate pH 6. Green: sodium phosphate pH 7. Yellow: Tris pH 8. Red: Tris pH 9. Black: protein standards - BSA (66.4 kDa) and soybean trypsin inhibitor (STI, 20.1 kDa), each at 0.5 mg mL^{-1}.

monomeric LbNOX (theoretical molecular weight: 51.1 kDa); (ii) a higher molecular-weight specie eluting earlier (around 12.5 mL), consistent with a dimeric form; (iii) and species eluting at around 11 mL, possibly corresponding to trimeric or tetrameric forms.

The proportion of these species varies with pH. At higher pH values, the monomeric form was favoured over the dimeric and multimeric forms. In contrast, at pH 6 and 7, the high-molecular weight species (likely trimer or tetramer) were more abundant. These species were prominent at pH 6, detectable at pH 7 in smaller amounts, and undetectable at pH 8 and 9. At pH 8, the solution contained both dimeric and monomeric forms, while at pH 9, the monomer was the predominant species.

To further characterise the distribution and heterogeneity of LbNOX oligomeric forms, size-exclusion chromatography coupled to multi-angle light scattering (SEC-MALS) was performed at pH values ranging from 5 to 9 (Table 2). The dimeric form was observed under all conditions, with its relative abundance increasing as the pH decreased down to pH 6, but decreasing again at pH 5. The monomeric form appeared from pH 7 onwards and became predominant at pH 9. Dimers, trimers and tetramers were detected at varying levels throughout the pH range, while higher-order multimeric species were only detected at pH 5, 6, and 7, and undetected at pH 8 and 9.

Table 2 summarizes the experimental molecular weights obtained for each SEC-MALS peak. The low polydispersity indices (1.002–1.027) observed for all peaks further confirm the high resolution and monodispersity of the detected oligomeric forms. The corresponding chromatograms are provided in Supplementary Material.

Among the tested conditions, pH 6 yielded the most

Table 2
Mass distribution profiles determined by SEC-MALS analysis.

Buffer condition	monomer	dimer	Trimer	tetramer	Higher multimeric forms
pH 5		110.5 kDa **55.3 %** 1.011	181.9 kDa 11.1 % 1.005	260.1 kDa 25.8 % 1.021	437.8 kDa 7.8 % 1.006
pH6		96.57 kDa **71.2 %** 1.002	142.9 kDa 7.2 % 1.003	221.3 kDa 18.4 % 1.027	387.6 kDa 3.2 % 1.003
pH 7	64.54 kDa **36.2 %** 1.006	99.44 kDa **33.5 %** 1.003	145.1 kDa 19.9 % 1.011	208.3 kDa 7.2 % 1.006	288.6 kDa 3.2 % 1.006
pH 8	51.61 kDa **44.4 %** 1.003	101.1 kDa **43.1 %** 1.004	158.3 kDa 9.4 % 1.006	213.6 kDa 3.1 % 1.005	
pH 9	51.82 kDa **67.0 %** 1.005	96.67 kDa 25.4 % 1.007	150.1 kDa 5.5 % 1.003	197.5 kDa 2.1 % 1.004	

Caption: Experimental molecular masses and polydispersity indices (Mw/Mn) of LbNOX oligomeric species determined by SEC-MALS. For each detected peak, the molecular weight (top value, in kDa), relative abundance (in %), and polydispersity index (bottom value) are indicated. Relative abundances in bold indicate the predominant species under each condition. Mw/Mn values between 1.000 and 1.050 are considered highly indicative of monodisperse species in SEC-MALS analysis.

homogeneous LbNOX sample, with a predominant dimeric form representing over 70 % of the total population and limited presence of larger oligomers. The pH 9 sample showed a comparable level of homogeneity but consisted mainly of monomeric form representing 67 % of the total population. The pH 5 sample, while relatively homogeneous, exhibited a higher proportion of trimeric, tetrameric and larger species. In contrast, the phosphate buffer at pH 7 led to a more heterogeneous profile, with a broad distribution of oligomeric states.

Fig. 6 illustrates the isoform relative percentages obtained for each tested pH condition.

3.4. Enzymatic activity of the LbNOX requires dimerisation and the presence of FAD

To determine whether LbNOX enzymatic activity is associated with specific oligomeric states, fractions corresponding to the different multimeric forms eluted from SEC were collected and analysed. UV–visible spectra were recorded to monitor protein content and FAD presence. Enzymatic activity was then measured on 1 µL of each fraction by following NADH consumption, in sodium phosphate buffer pH 7, with or without addition of 25 µM FAD, to correlate activity profiles with elution peaks.

These data indicate that, in the absence of supplemented FAD, the LbNOX monomeric form is inactive and only the dimeric form exhibits enzymatic activity (solid black lines in Fig. 7). UV–visible spectra of the collected fractions confirm the presence of FAD in the dimeric form but not in the monomeric form (data not shown). Upon addition of exogeneous FAD, the monomeric fractions become enzymatically active (dotted black lines in Fig. 7). In the absence of supplemented FAD, the enzymatic activity of the dimeric form is comparable at pH 7, 8 and 9 (33, 36 and 35 µmol min^{-1}, respectively), but markedly higher at pH 6 (53 µmol min^{-1}). In the presence of FAD, the dimeric form shows enhanced activity at pH 6 and 7 (147 and 97 µmol min^{-1}, respectively), while activity remains similar at pH 8 and pH 9 (53 and 31 µmol min^{-1}). At these higher pH values, the predominantly monomeric enzyme also becomes active in the presence of supplemented FAD. In all tested conditions, the fractions corresponding to trimeric and tetrameric forms also displayed

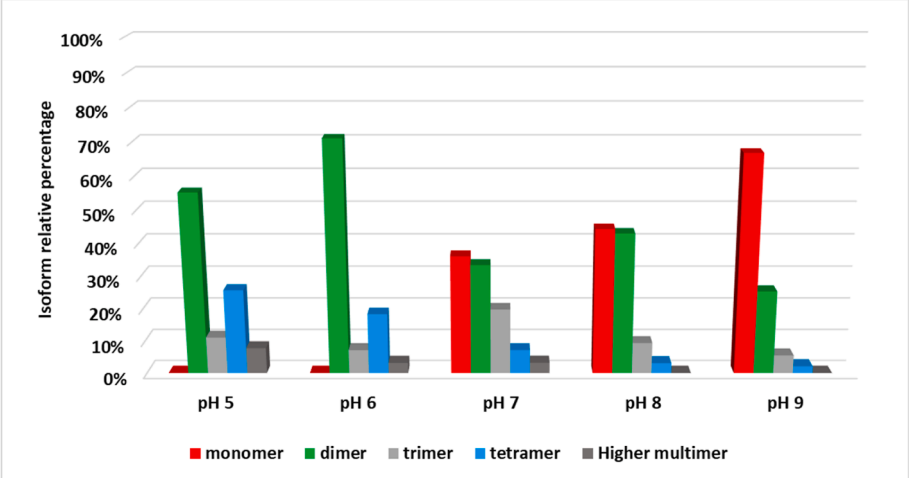

Fig. 6. Relative proportions of LbNOX isoforms determined by SEC–MALS under different buffer conditions. Bars represent the percentage distribution of each isoform across a pH range 5–9. Colours indicate the oligomeric states: monomer (red), dimer (green), trimer (light grey), tetramer (blue), and higher-order multimers (dark grey).

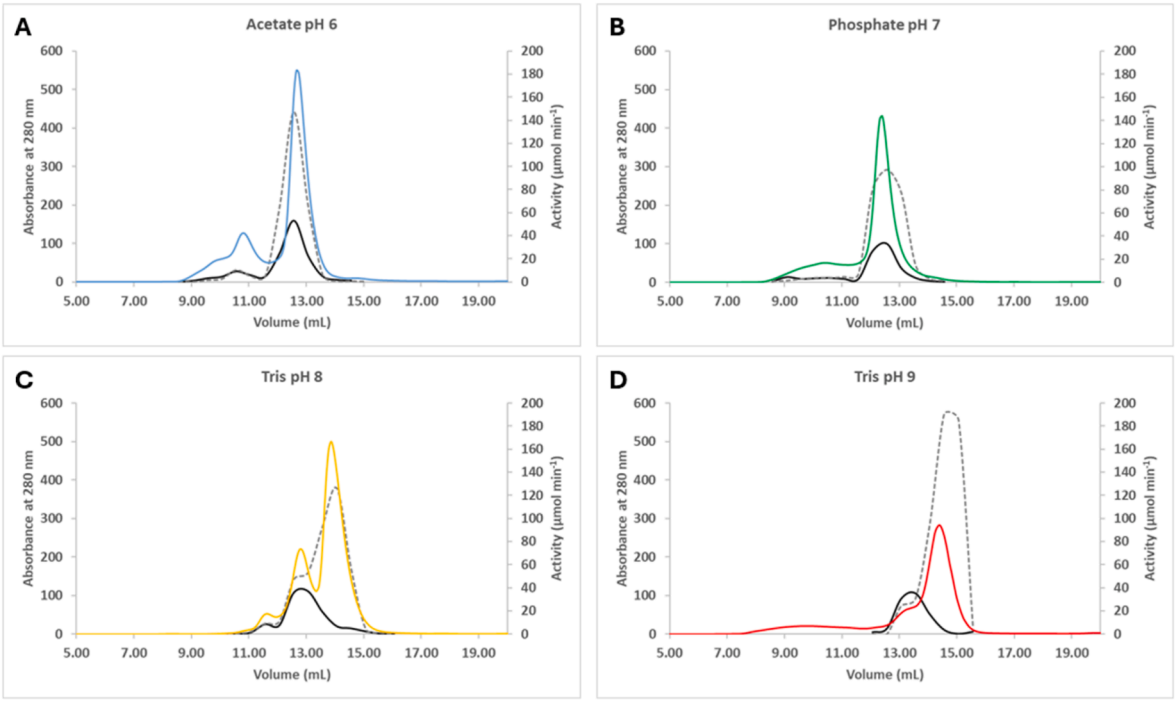

Fig. 7. LbNOX activity of SEC-eluted fractions under different buffer conditions. All buffers contained 50 mM buffer (acetate, phosphate or Tris) and 150 mM NaCl. **A.** acetate, pH 6. **B.** phosphate, pH 7. **C.** Tris, pH 8. **D.** Tris, pH 9. The X-axis shows the elution volume (mL). The left Y-axis shows the absorbance at 280 nm. The right Y-axis shows the enzymatic activity (in µmol min^{-1}). Coloured lines correspond to the absorbance at 280 nm, solid black lines correspond to LbNOX activity, and grey dotted lines to LbNOX activity in the presence of 25 µM FAD.

enzymatic activity, indicating that these higher-order oligomers retain catalytic function.

3.5. The role of pH and FAD in the structure of LbNOX

To better understand the influence of FAD on the oligomeric state and enzymatic activity of LbNOX, the apoenzyme (1 mg mL^{-1}) was prepared using two consecutive SEC runs in Tris buffer at pH 9. High-pH conditions were shown to favour the monomeric form of LbNOX (Fig. 5). The collected fractions displayed no detectable activity, and UV–visible spectra confirmed the absence of FAD (data not shown). This protein sample preparation is hereafter referred to as “apoLbNOX”.

To investigate whether pH or the presence of FAD influences LbNOX dimerisation, apoLbNOX was subjected to an additional SEC run equilibrated in acetate buffer at pH 6, a condition known to promote the dimeric form of LbNOX. This experiment was performed both with and without 2.5 µM FAD (Fig. 8A). UV–visible spectra were recorded to monitor protein content. Enzymatic activity was then measured on 1 µL of each fraction by following NADH consumption, in sodium phosphate buffer pH 7, to correlate activity profiles with elution peaks.

Fig. 8A shows that the apoLbNOX sample was converted into a dimer (retention volume of 12.3 mL) when subjected to SEC in acetate buffer at pH 6, consistent with previous results (Fig. 5). However, in the absence of supplemented FAD, the peak corresponding to the dimeric LbNOX displays a broad and asymmetric profile, with a significant tail indicating the presence of higher-order oligomers. Moreover, this dimeric apoenzyme remains inactive due to the lack of FAD. These data indicate that dimerisation can occur independently of FAD, but is not sufficient to restore enzymatic activity (Fig. 8B); FAD must be supplemented to enable efficient NADH oxidation. As expected, the addition of 2.5 µM FAD to the apoLbNOX sample during the SEC experiment fully restores enzymatic activity (Fig. 8C). The active form of LbNOX appears essentially dimeric (retention volume 12.4 mL), with a sharper and more symmetrical elution profile compared to the FAD-free dimer.

The effect of FAD on the quaternary structure of purified LbNOX was further analysed by SEC-MALS in phosphate buffer (pH 7) and Tris buffer (pH 9), both supplemented with 2.5 µM FAD (Table 3). The experiment aimed to determine whether FAD could reproduce the beneficial effect on sample homogeneity previously observed in acetate buffer at pH 6.

Fig. 9 illustrates the isoform percentages obtained for each tested condition.

The data show that in phosphate buffer at pH 7, where the monomeric and dimeric form of LbNOX were expected to be present in comparable proportions, the addition of 2.5 µM FAD shifts the equilibrium towards the dimeric form, significantly improving the homogeneity of the enzyme solution. In contrast, the SEC-MALS profile obtained in Tris buffer at pH 9 indicates that the enzyme remains predominantly monomeric, with only a minor fraction forming stable dimers, which is comparable to the profiles observed without supplemented FAD. Interestingly, two distinct dimeric peaks with calculated masses of 92.9 kDa and 109.3 kDa appear at pH 9 in the presence of FAD, suggesting the existence of two enzyme isoforms under this condition. The mass difference (16.4 kDa) cannot be explained solely by the presence of FAD (0.8 kDa), but it is possible that FAD binding alters the protein's refractive index, which could affect mass determination unless corrected for the exact refractive index of the apo- and holo-forms. In conclusion, the monomeric form is strongly favoured at high pH values, and FAD supplementation alone is insufficient to promote dimerisation. However, at near-neutral pH, the addition of FAD significantly improves ample homogeneity, with the dimeric form becoming predominant.

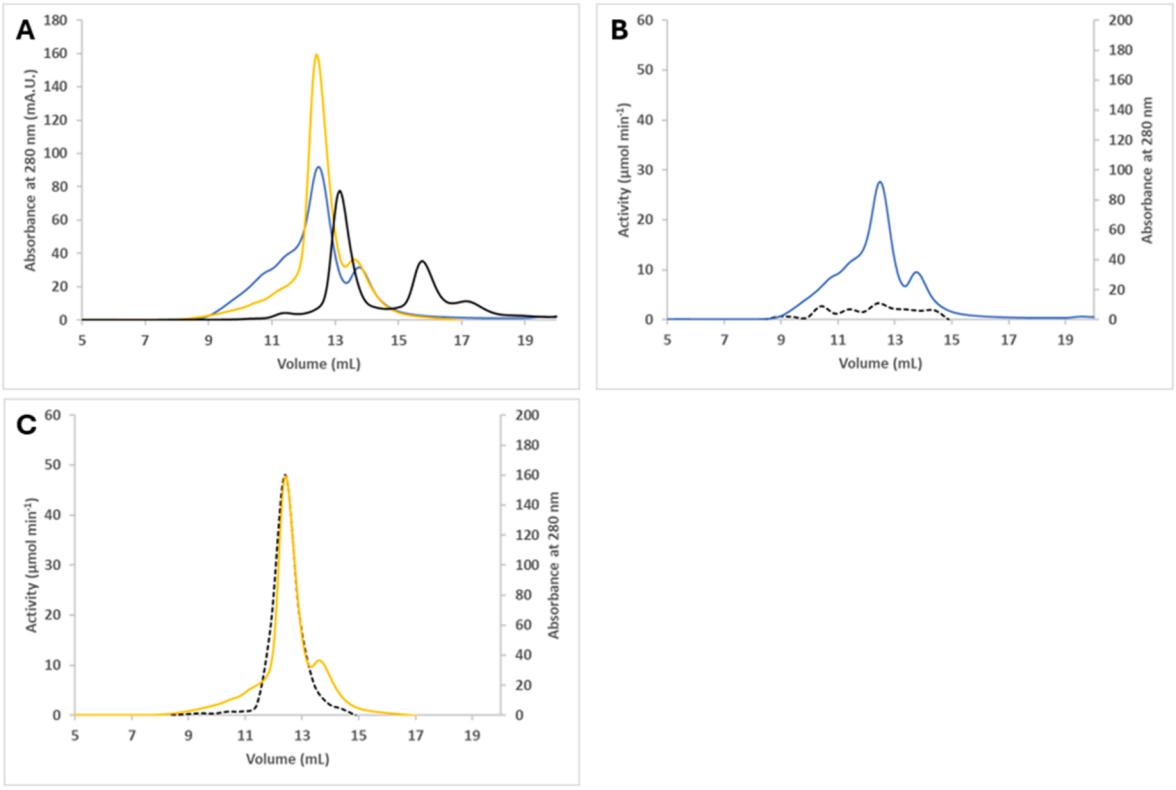

Fig. 8. Size-exclusion chromatograms and enzymatic activity of apoLbNOX. **A.** Size-exclusion chromatograms of apoLbNOX in 50 mM acetate, 150 mM NaCl, pH 6, with or without 2.5 μM FAD. The X-axis represents the elution volume (mL) and the Y-axis shows absorbance at 280 nm (mA U.). Blue: ApoLbNOX in acetate buffer pH 6. Yellow: ApoLbNOX in acetate buffer pH 6 supplemented with 2.5 μM FAD. Black: standard mixture of BSA (66.4 kDa) and STI (20.1 kDa), each at 0.5 mg mL^{-1}. **B.** Chromatogram (blue line) and enzymatic activity (black dotted line, μmol min^{-1}) of apoLbNOX in acetate buffer pH 6. **C.** Chromatogram (yellow line) and enzymatic activity (black dotted line, μmol min^{-1}) of the apoLbNOX in acetate buffer pH 6 supplemented with 2.5 μM FAD.

Table 3
Mass profiles obtained by SEC-MALS analysis.

Buffer condition	monomer	dimer	trimer	tetramer	Hexamer
pH 7.0	64.54 kDa **36.2 %**	99.44 kDa **33.5 %**	145.1 kDa 19.9 %	208.3 kDa 7.2 %	288.6 kDa 3.2 %
pH 7.0 2.5 μM FAD	62.75 kDa 3.6 % 1.002	96.30 kDa **70.9 %** 1.005	148.6 kDa 10.8 % 1.009	191.9 kDa 14.7 % 1.012	
pH 9.0	51.82 kDa **67.0 %**	96.67 kDa 25.4 %	150.1 kDa 5.5 %	197.5 kDa 2.1 %	
pH 9.0 2.5 μM FAD	54.33 kDa **73.6 %** 1.008	92.95 kDa 13.3 % 1.004 109.3 kDa 10.6 % 1.005		194.3 kDa 2.4 % 1.026	

Caption: Experimental molecular masses and polydispersity indices (Mw/Mn) of LbNOX oligomeric species determined by SEC-MALS. For each detected peak, the molecular weight (top value, in kDa), relative abundance (in %), and polydispersity index (bottom value) are indicated. Relative abundances in bold indicate the predominant species under each condition. Mw/Mn values between 1.000 and 1.050 are considered highly indicative of monodisperse species in SEC-MALS analysis.

3.6. Characterization of the LbNOX enzymatic activity

3.6.1. Determination of the optimum pH for activity

Given the influence of pH and FAD supplementation on LbNOX oligomerisation and homogeneity, the optimum pH for LbNOX activity was determined. Fig. 10 shows the mean values and standard deviations from three independent replicates.

The maximum activity of the enzyme is observed at pH 6. Below this value, the activity of the enzyme drops markedly, whereas above pH 6 the rate of oxidation also decreases but more gradually. This result correlates with the observation (Fig. 5) that pH 6 promotes the dimeric form of LbNOX which corresponds to its active form.

3.6.2. Effect of FAD addition on the LbNOX activity

Building on the influence of pH and oligomerisation on LbNOX activity, we next examined how varying concentrations of FAD affect the enzyme's catalytic performance (Fig. 11).

As expected, the data show a marked increase in the rate of NADH oxidation with increasing FAD concentrations, reaching a plateau at around 2.5 μM FAD. Hanes-Woolf regression plot was used to determine the Michaelis constant (K_M), which can be considered equivalent to the equilibrium association constant value (K_D) for the non-covalent interaction between LbNOX and FAD. The fitted K_M (K_D) value is 0.257 μM, which is comparable to the K_D values reported for other enzymes that use FAD as cofactor [24]. The fitted k_{cat} value is 1.63 s^{-1}. Affinity parameters were determined at 20 °C. While temperature can influence K_D values, such effects are generally modest for small, stable enzyme–cofactor interactions like that between FAD and LbNOX, particularly when measurements are carried out near ambient temperatures, commonly used in binding studies [25].

Furthermore, based on the specific activity measurements (expressed as μmol of NADH oxidised per minute per μg of LbNOX) and the concentration of FAD supplemented in the enzymatic

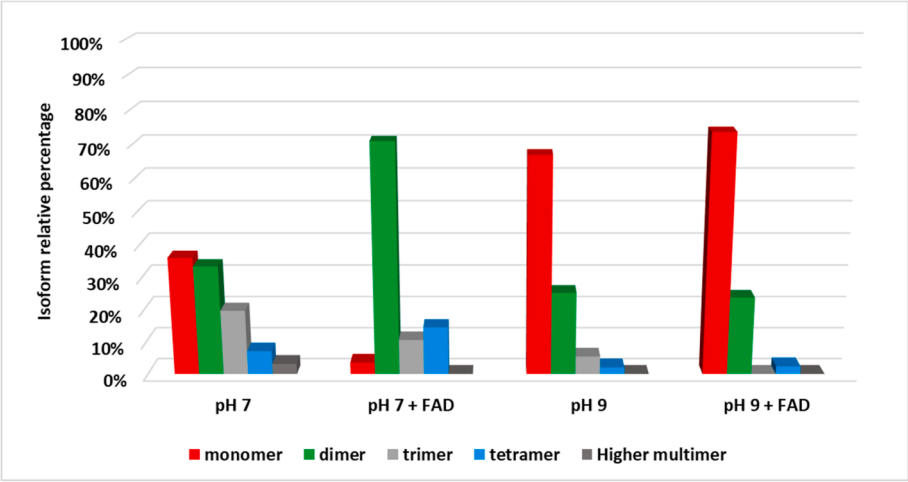

Fig. 9. Relative proportions of LbNOX oligomeric isoforms determined by SEC–MALS at pH 7 or pH 9 with or without 2.5 μM FAD. Bars represent the percentage distribution of each isoform under each condition. Colours indicate the oligomeric states: monomer (red), dimer (green), trimer (light grey), tetramer (blue), and higher-order multimers (dark grey).

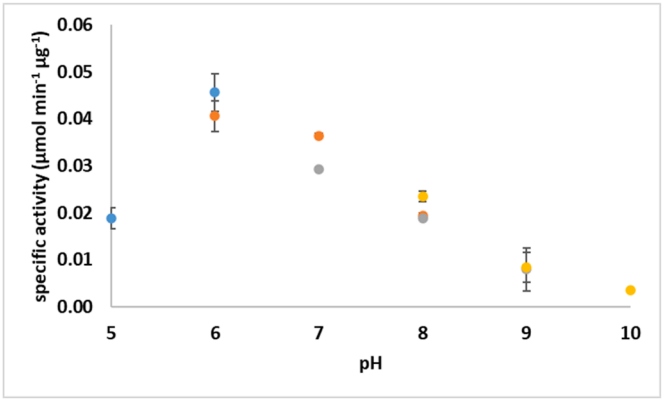

Fig. 10. LbNOX specific activity as a function of pH. Activity was measured in buffers containing 150 mM NaCl and 50 mM buffer. Blue dots: acetate; orange dots: phosphate; grey dots: Tris; yellow dots: glycine.

reaction, we estimated that about 30 % of the LbNOX present in the purified enzyme preparation was active without any supplemented FAD. The percentage of active protein was calculated as: % of active protein = (specific activity without supplemented FAD/ specific activity with FAD) x 100 = (0.013/0.051) x 100 = 25.5 %.

3.6.3. Determination of the catalytical parameters of the LbNOX for its substrate (NADH) in the presence/absence of its supplemented cofactor (FAD)

In these assays we wanted to identify the best experimental conditions to maximize the enzymatic activity of the purified LbNOX. The catalytic parameters of the enzyme for NADH were determined in three conditions: a) LbNOX (not activated) without FAD in the reaction buffer; b) LbNOX with FAD supplemented in the reaction buffer; and c) FAD-activated LbNOX without FAD in the reaction buffer. The data (average values) are summarized in Table 4. Michealis-Menten graphs and Hanes-Woolf plots are provided in Fig. 12.

The data show that FAD-activation improves the catalytic properties of LbNOX. The FAD-activated enzyme exhibits a markedly lower K_M value (33.12 μM) compared with the non-activated enzyme (48.37–59.12 μM), consistent with a higher apparent affinity for NADH. In contrast, when FAD is added only to the reaction buffer, K_M increases slightly, suggesting a modest reduction in NADH affinity under these conditions.

With respect to turnover, the catalytic constant (k_{cat}), and consequently the catalytic efficiency (k_{cat}/K_M), increase substantially in the presence of FAD. Supplementing FAD directly in the reaction buffer results in an approximately twofold increase in k_{cat} (2.97 s^{-1} vs 1.36 s^{-1}), while pre-activation of the enzyme with FAD leads to nearly a fivefold enhancement (4.97 s^{-1}). Consequently,

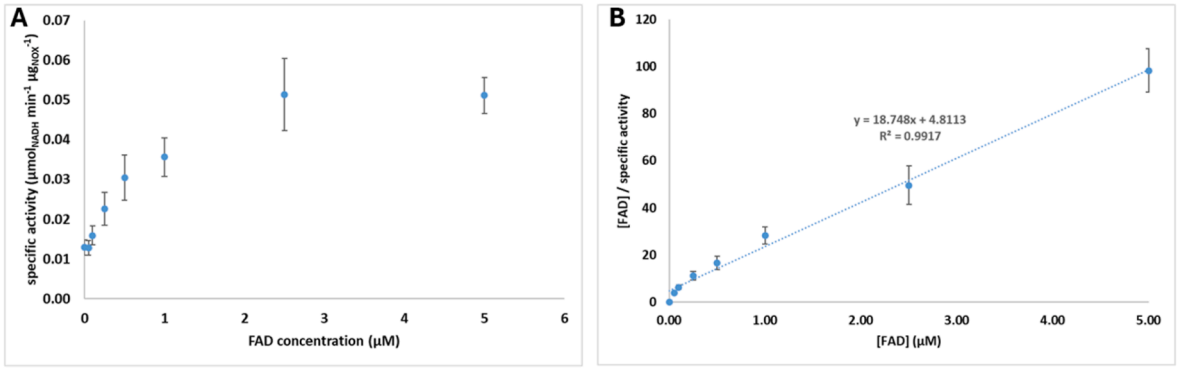

Fig. 11. A. LbNOX specific activity as a function of FAD concentration. **B.** Hanes-Woolf plot.

Table 4
Catalytic parameters for the different experimental conditions.

Parameter	LbNOX not FAD-activated, no FAD in the activity assay	LbNOX not FAD-activated, 2.5 μM FAD in the activity assay	LbNOX FAD-activated, no FAD in the activity assay
Vmax	0.03 μM s-1 (0.025–0.030)	0.06 μM s-1 (0.055–0.065)	0.10 μM s-1 (0.088–0.113)
K_M	48.37 μM (43.88–52.15)	59.12 μM (55.71–62.00)	33.12 μM (18.87–51.42)
k_{cat}	1.36 s-1 (1.26–1.49)	2.97 s-1 (2.74–3.24)	4.97 s-1 (4.42–5.67)
k_{cat}/K_M	0.03 μM-1 s-1 (0.024–0.034)	0.05 μM-1 s-1 (0.044–0.058)	0.15 μM-1 s-1 (0.110–0.234)

Caption: Vmax is calculated for 20 nM LbNOX. In brackets: 95 % confidence interval values calculated based on linear regression model of Hanes-Woolf plot.

the catalytic efficiency rises from 0.03 μM^{-1} s^{-1} in the non-activated state to 0.15 μM^{-1} s^{-1} after FAD activation. These catalytic parameters are in the same order of magnitude as those previously reported for water forming NADH oxidases [26,27].

Altogether, the results strongly support that pre-activation with FAD is the most effective way to obtain a fully active enzyme. This likely reflects the fact that prolonged incubation with FAD allows efficient diffusion and tight binding of the cofactor within the dimeric form of LbNOX. Moreover, activation with 2.5 μM of FAD appears sufficient to saturate the active sites, as no further increase in enzymatic velocity is observed when additional FAD is supplied in the reaction buffer of the assay (data not shown).

3.7. Stability analysis

As LbNOX activity is pH dependent and closely linked to its

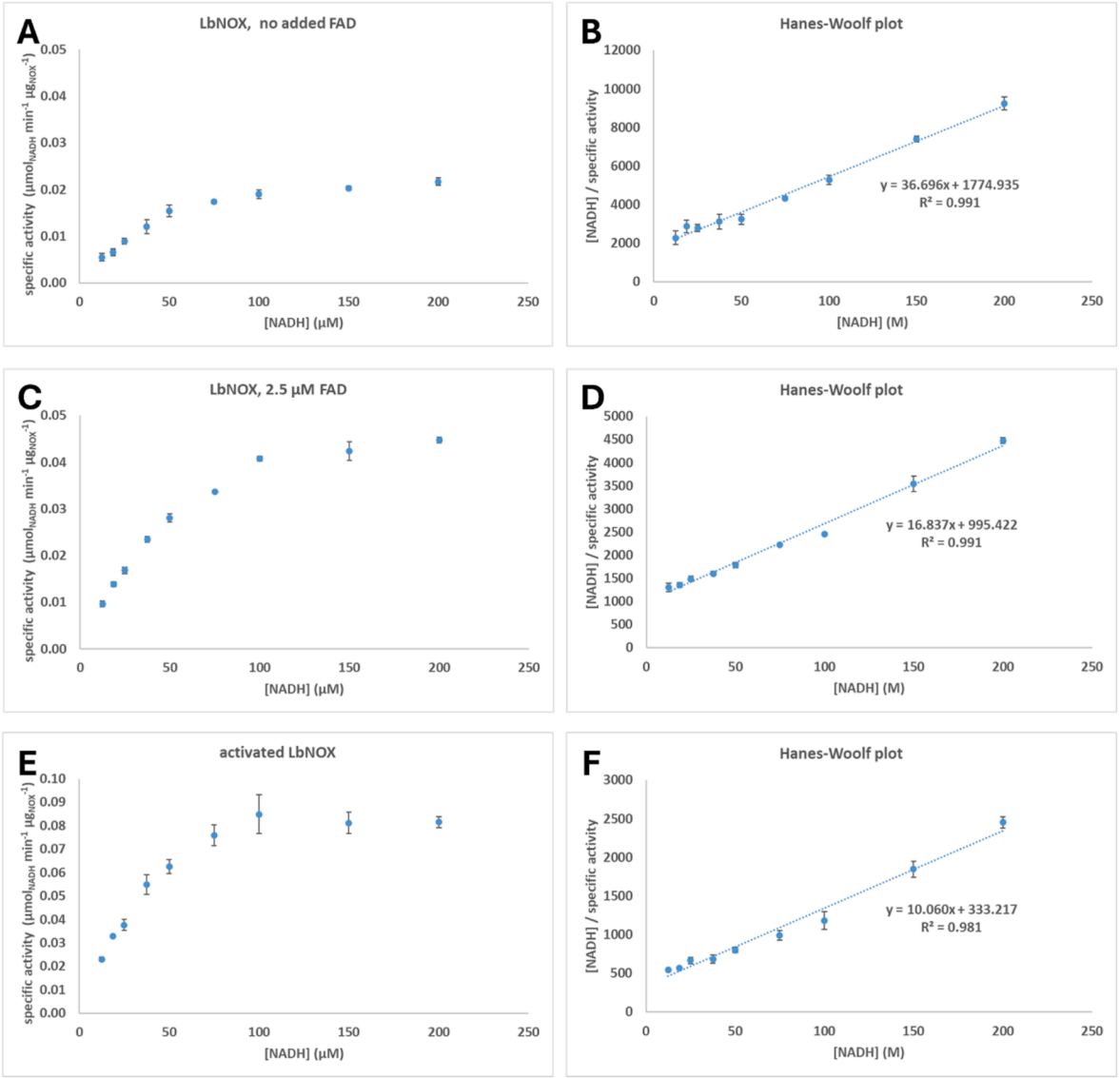

Fig. 12. Catalytic parameters determined in experimental conditions **A.** LbNOX (not activated) without FAD in the activity assay buffer. **B**. Same as precedent, Hanes-Woolf plot. **C** LbNOX (not activated) with 2.5 μM FAD supplemented in the activity assay buffer. **D**. Same as precedent, Hanes-Woolf plot. **E.** FAD-activated LbNOX without FAD in the activity assay buffer. **F**. Same as precedent, Hanes-Woolf plot.

dimerisation, the stability of the protein across different pH conditions was investigated. Stability was assessed using a formulation screen covering 158 different buffer solutions spanning pH 2 to 10 [15], followed by Differential Scattering Fluorimetry (DSF) analysis to determine the melting temperature (T_m) in each condition [28] (Fig. 13).

The data indicate that the optimal stability of LbNOX occurs around pH 6, where the highest T_m values are observed (43.25 °C in acetate pH 6.1 and citrate pH 5.9). The lowest T_m values are observed at pH 4.5, and no T_m could be measured below this point, consistent with complete denaturation under highly acidic conditions. T_m increases between pH 4.5 and 6, then decreases to a minimum around pH 8, followed by a slight rise at more alkaline pH. However, since alkaline conditions favour the inactive monomeric form of the protein, high pH values should be avoided for LbNOX formulation.

The stability of the LbNOX in acetate buffer pH 6.0 is also confirmed by DSC (Differential Scanning Calorimetry) (data not shown, $T_m = 43.4$ °C) and correlates very well with the T_m value obtained in the formulation experiment for acetate pH 6.1 ($T_m = 43.25$ °C).

3.8. Structural analysis

As pH influences both the quaternary structure of LbNOX and its interaction with FAD, we examined the 3D structure to identify charged residues at the dimer interface whose side chain protonation states could be pH-dependent. Interfaces between monomers were identified by the PISA software [16]. PISA analysis of the structure (PDB ID: 5VN0) shows that the dimer interface is highly specific, with strong shape and charge complementarity. The calculated free energy of dimerisation is $\Delta^iG = -35.5$ kcal mol^{-1}, and the associated P-value is 0.005. By contrast, interactions between dimers forming higher-order oligomers (e.g. tetramers) are non-specific, with no predicted hydrogen bonds and much lower Δ^iG values. At the dimer interface, 36 hydrogen bonds are identified, involving 20 residues in each monomer. Notably, 11 of these hydrogen bonds involve the side chains of 4 charged residues: Glu161, Arg302, Asp394, and Asp419. The atom–atom details of these hydrogen bonds, as determined by PISA, are provided in Supplementary Material.

Since previous data indicate that the quaternary structure of LbNOX is pH dependent and given that pH can affect the protonation state of charged residues, it is likely that changes in the protonation state of interfacial residues account for the observed transition from the dimeric to the monomeric form. To test this hypothesis, the monomeric and the dimeric structures, with and without cofactors (FAD and O_2), were analysed using the PDB2PQR-APBS software [18] to obtain the pKa values of the residues that are part of the dimerisation interface. The results are highly consistent across the different force field. The main shifts of pKa values are summarized in Table 5.

Changes in pKa values at the dimerisation interface are not uniformly small. Several residues show meaningful shifts upon dimerisation: Asp394 increases by ~2 pH units (from 2.84 to 2.85 in the monomer to 4.69–5.05 in the dimer), Glu161 shifts into the 7–8 pH range (from 6.76 to 7.32 to 7.06–7.79), Asp419 increases modestly (from 3.98 to 4.46–4.50), and Arg302 decreases (from

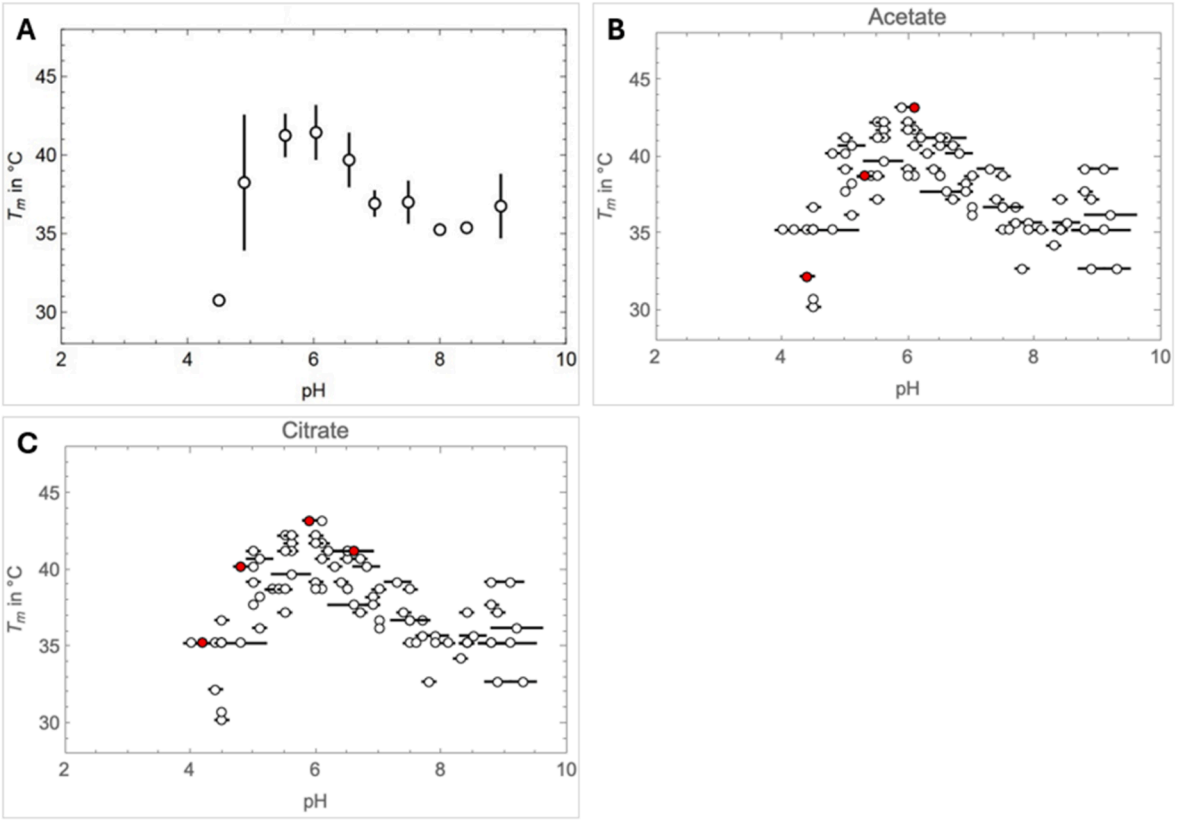

Fig. 13. High throughput formulation screen using DSF. X axis: pH values. Y axis: T_m (°C). **A.** Data points represent average T_m obtained for each 0.5 pH unit across all tested buffers, with vertical error bars indicating standard deviations. **B. and C.** Empty circles show T_m values for all individual conditions. Red circles represent the Tm values obtained for (B) acetate buffer at pH 4.4, 5.3 and 6.1 and (C) citrate buffer at pH 4.2, 4.8, 5.9 and 6.6.

Table 5
PKa values for monomeric and dimeric isoform of LbNOX with and without cofactors.

Residue #	5VN0 monomer without cofactors	5VN0 monomer with cofactors	5VN0 dimer without cofactors	5VN0 dimer with cofactors
Residues at dimerisation interface				
Asp394	2.84	2.85	5.05–4.69	5.05–4.69
Asp419	3.98	3.98	4.46–4.47	4.49–4.50
Glu161	6.76	7.32	7.45–7.06	7.79–7.41
Arg302	12.00	11.92	10.36–10.39	10.34–10.36
Other residues				
Asp427	4.70	4.70	8.46–8.60	8.51–8.65
Cys42	10.11	10.35	13.01–12.84	13.16–12.99

Caption: for the dimer, two pKa values are indicated, one per chain (i.e. A chain - B chain).

11.92 to 12.00 to 10.34–10.39). Among these, the shift of Glu161 places its pKa close to the experimental transition window (pH 7–8), making it a plausible contributor to the pH-driven shift from the dimeric to the monomeric form. By contrast, although the Asp394 shift is sizeable, its pKa remains well below neutrality, so the residue is expected to be deprotonated at pH 7–9 and is less likely to be the primary driver of the transition.

In the rest of the protein, notable shifts are observed for two residues: Cys42 and Asp427. Interestingly, Cys42 is critical for enzyme activity, as it is directly involved in the catalytic reaction [12]. Therefore, a change of its pKa could directly impact the enzymatic rate of LbNOX. Asp427 is neither part of the dimerisation interface nor of the catalytic pocket. It is located behind the loop formed by Phe422, Gln423 and Pro424, which closes the catalytic pocket on the opposite monomer (Fig. 14). Asp427 forms hydrogen bonds with Leu421 (Asp427[HOD2]–Leu421[O]), Gln423 (Asp427[OD1]–Gln423[N] and Asp427[N]–Gln423[O]) and Asn431 (Asp427[OD2]–Asn431[ND2]), contributing to the stability of the dimerisation interface. Gln423, in turn, forms a hydrogen bond with Glu161 of the opposite monomer (Gln423[NE2]–-Glu161[OE2]). In the 5VN0 structure, the extremity of the Glu161 side chain is involved in H-bonds with two water molecules and the extremity of the Asp427 side chain makes one H-bond with a water molecule. These water molecules are located in cavities connected to the solvent through channels, making these residues sensitive to pH-dependent changes.

Structures with the appropriate protonation states at different pH values were generated using the PDB2PQR-APBS software. Due to its pKa shift, Asp427 is protonated at OD2 in the dimer between pH 5 and 8, but remains deprotonated in the monomer at all pH values. As illustrated in Fig. 14, protonation of Asp427 is essential for the formation of the hydrogen bond with Leu421. For Glu161, its protonation state could modulate the local H-bond network, rather than act as an absolute switch.

Within the catalytic pocket, Glu32 and Asp279, which interact with the FAD cofactor, are protonated at pH 5 and 6 but not at higher pH values. The active residue Cys42 remains unprotonated across the entire pH range. Protonated structures at pH 6 and 9 are provided in Supplementary Material.

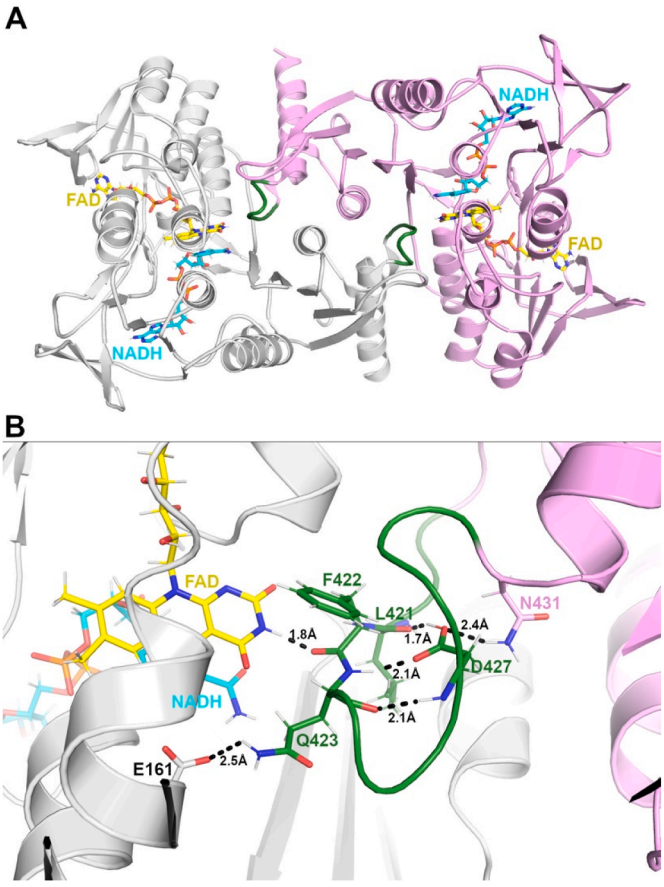

Fig. 14. Asp427 the best candidate for the pH dependent dimer to monomer transition. **A.** Cartoon representation of the LbNOX dimer (PDB ID 5VN0, after protonation state calculation with APBS at pH 6), with monomer A in grey and B in pink. FAD and NADH are displayed as yellow and cyan sticks, respectively. The Asp427 bearing loop is shown in green. **B.** Close-up view of the Asp427 containing loop with residues of interest shown as green sticks. Hydrogen bonds formed between Asp427 and the neighbouring residues are displayed as black dashed lines, as well as the hydrogen bond of Phe422 with FAD.

4. Discussion

4.1. The LbNOX activity is associated with the dimeric isoform

Our kinetic assays revealed an intriguing effect of FAD on substrate affinity: the apparent affinity for NADH decreased (higher K_M) when FAD was present in the reaction buffer. This observation suggests that LbNOX may operate through more than one mechanistic pathway, consistent with the catalytic model proposed by Argyrou & Blanchard.

More broadly our results demonstrate that LbNOX activity is associated with the dimeric isoform and the presence of FAD. This observation is consistent with the crystal structure of LbNOX [11], as well as those of water forming NADH oxidases from other organisms [29,30]. We also demonstrated that the abundance of the dimeric isoform is strongly pH-dependent: it predominates at pH 6, which corresponds to the optimal pH for both LbNOX activity and stability. In contrast, the monomeric isoform observed at alkaline pH results in an inactive enzyme that is unable to retain the FAD cofactor. These observations are in line with the acidic pH

values generally required for water-forming NADH oxidases [31–33], although exceptions exist where optimal activities occur at neutral to alkaline pH [26,27]. Moreover, alkaline conditions are unfavourable for the formation of the sulfonic acid (Cys-SOH) intermediate, further contributing to the loss of activity.

Interestingly, FAD is not strictly required for dimerisation. Indeed, an inactive dimeric apoenzyme was observed when the apo-monomer was formulated in acetate buffer at pH 6 (Fig. 8). The presence of a dimeric apoprotein under acidic conditions has previously been reported for *Thermus thermophilus* NADH oxidase [34] (Uniprot accession number: Q60049). This observation is consistent with the fact that LbNOX purification leads to a heterogeneous protein solution that is not fully active. Only a small fraction of the LbNOX molecules contains FAD (17.5 %), but full activation (corresponding to an approximately fourfold increase of the enzymatic activity) can be achieved by incubating the enzyme with FAD. Furthermore, addition of FAD at pH 6 or 7 enhances homogeneity of the enzyme solution by increasing the relative proportion of the dimeric isoform, suggesting that FAD stabilizes the quaternary structure of LbNOX. However, FAD alone cannot induce LbNOX dimerisation at higher pH values, likely due to charge changes on the side chains of residues involved in oligomerisation.

Overall, these data indicate that FAD stabilizes the quaternary structure of LbNOX, with the dimeric isoform being necessary to imprison FAD, although the binding remains reversible. It should be noted that the influence of ionic strength on LbNOX quaternary structure was not experimentally addressed, but the salt concentration used were comparable to those reported in previous studies [10,11].

The activity of higher-order multimers was not characterised in this study, as these assemblies are less stable and mainly mediated by hydrophobic interactions. Their oligomerisation therefore appears to be a dynamic process, modulated by pH and cofactor occupancy, suggesting a delicate equilibrium between structural stability and catalytic competence.

4.2. Critical residues for LbNOX quaternary structure

The FAD cofactor is located inside the catalytic pocket of one monomer, which is closed by a loop from the opposite monomer, making the dimeric isoform mandatory to efficiently retain the cofactor. In the 5VN0 structure, the B-factors of the FAD atoms are very similar to those of the surrounding protein residues, which strongly suggests a high occupancy, likely close to 100 %. Structural inspection suggests that the entry site for FAD into the catalytic pocket is located at the dimerisation interface. This observation implies the existence of a dynamic equilibrium between the monomeric and dimeric forms of LbNOX, which would enable transient opening of the catalytic pocket that allows FAD to enter each monomer.

The dimeric isoform is maintained through a network of interactions between atoms from the dimerisation interface and with atoms from other residues. Since the monomeric isoform predominates at pH 8, we initially hypothesised that histidine residues might play a role in the dimerisation process. However, sequence and structural analyses indicated that no histidine is located at the dimer interface. Instead, these analyses highlighted Asp427, whose pKa is strongly modulated by the oligomeric state of LbNOX, despite not being directly part of the dimerisation interface. Another observation is that protonation of Asp427 at OD2 is mandatory to establish the hydrogen bond with Leu421, thereby positioning residues Phe422, Gln423 and Pro424 to close the catalytic pocket from the opposite monomer. Shifting the position of Gln423 could prevent hydrogen bonding with Glu161 of the opposite monomer (protonated at OE2 at acidic pH), which undergoes deprotonation at alkaline pH values.

Together, these observations suggest that the protonation state of Asp427 at alkaline pH could explain the experimentally observed monomeric apoform of LbNOX. Supporting this hypothesis, sequence alignments with other water-forming NADH oxidases show that the four residues involved in this hydrogen-bonding network (Asp427, Leu421, Gln423 and Glu161) are strictly conserved (see supportive data).

5. Conclusion and insights

This study highlights the strict dependence of LbNOX activity on its dimeric isoform and on the presence of the FAD cofactor. This oligomeric state is strongly influenced by pH but does not necessarily correlate with activity, as inactive dimeric apoenzyme can be observed. These findings emphasise that formulation parameters must be carefully controlled, since they critically affect structural conformation, cofactor retention, and stability. Because recombinant production of LbNOX yields heterogeneous protein solutions, rigorous analytical monitoring is essential. SEC-MALS should be employed to assess homogeneity, specific absorbance peaks to verify FAD incorporation, and activity assays with and without cofactor to verify full activation.

Beyond LbNOX, this work illustrates how combining structural and functional analyses can be combined to define the conditions governing stability and activity in dimeric, flavin-dependent oxidoreductases. Our findings thus provide a type-example for the optimisation of related enzymes in cofactor regeneration systems. More generally, the approach described here is applicable to multimeric and cofactor-dependent oxidoreductases, helping to improve their stability and activity for industrial applications.

CRediT authorship contribution statement

Mathieu Dondelinger: Writing – original draft, Methodology, Formal analysis, Conceptualization. **Marylène S. Vandevenne:** Writing – review & editing, Formal analysis. **Frédéric Kerff:** Writing – review & editing, Formal analysis. **Moreno Galleni:** Writing – review & editing, Supervision, Conceptualization.

Funding sources

This research was financially supported by the European Regional Development Fund (ERDF) and Wallonia in the framework of the operational program “Wallonia-2020.EU”.

Frederic Kerff is a Research Associate of the F.R.S.-FNRS.

Declaration of competing interest

None.

8. Acknowledgment

The authors thank Fabrice Bouillenne for his help with SEC-MALS experiments and Georges Feller for carrying out the DSC experiments. The authors acknowledge the Robotein® platform of the BE Instruct-ERIC Centre for providing access to the Microlab STAR liquid handling workstation that was used to perform the DSF experiments.

Appendix A. Supplementary data

Supplementary data to this article can be found online at https://doi.org/10.1016/j.biochi.2025.12.013.

References

[1] J. Liu, H. Li, G. Zhao, Q. Caiyin, J. Qiao, Redox cofactor engineering in industrial microorganisms: strategies, recent applications and future directions, J. Ind. Microbiol. Biotechnol. 45 (5) (2018) 313–327, https://doi.org/10.1007/s10295-018-2031-7.

[2] H. Zhao, W.A. van der Donk, Regeneration of cofactors for use in biocatalysis, Curr. Opin. Biotechnol. 14 (6) (2003) 583–589, https://doi.org/10.1016/j.copbio.2003.09.007.

[3] Z. Zhang, X. Zhang, X. Ji, Developing and regenerating cofactors for sustainable enzymatic CO_2 conversion, Processes 10 (2) (2022) 230, https://doi.org/10.3390/pr10020230.

[4] K. Bachosz, J. Zdarta, M. Bilal, A.S. Meyer, T. Jesionowski, Enzymatic cofactor regeneration systems: a new perspective on efficiency assessment, Sci. Total Environ. 868 (2023) 161630, https://doi.org/10.1016/j.scitotenv.2023.161630.

[5] M. Xu, Z. Tan, C. Zhu, W. Zhuang, H. Ying, P. Ouyang, Recent advance of chemoenzymatic catalysis for the synthesis of chemicals: scope and challenge, Chin. J. Chem. Eng. 30 (2021) 146–167, https://doi.org/10.1016/j.cjche.2020.12.016.

[6] J. Rocha-Martín, D. Vega, J.M. Bolivar, C.A. Godoy, A. Hidalgo, J. Berenguer, J.M. Guisán, F. López-Gallego, New biotechnological perspectives of a NADH oxidase variant from Thermus thermophilus HB27 as NAD+-recycling enzyme, BMC Biotechnol. 11 (1) (2011) 101, https://doi.org/10.1186/1472-6750-11-101.

[7] Sakamoto, M.; Uchimura, T. Comparison of H_20-Forming NADH oxidase from Leuconostoc mesenteroides subsp. Mesenteroides NRIC 1541T and H202-Forming NADH Oxidase from Sporolactobacillus inulinus NRIC 1133T..

[8] X. Yang, K. Ma, Characterization of an exceedingly active NADH oxidase from the anaerobic hyperthermophilic bacterium *Thermotoga maritima*, J. Bacteriol. 189 (8) (2007) 3312–3317, https://doi.org/10.1128/JB.01525-06.

[9] B. Petschacher, N. Staunig, M. Müller, M. Schürmann, D. Mink, S. De Wildeman, K. Gruber, A. Glieder, Cofactor specificity engineering of Streptococcus mutans NADH oxidase 2 for NAD(P)+ regeneration in biocatalytic oxidations, Comput. Struct. Biotechnol. J. 9 (14) (2014) e201402005, https://doi.org/10.5936/csbj.201402005.

[10] J. Zhang, Z. Cui, H. Chang, X. Fan, Q. Zhao, W. Wei, Conversion of glycerol to 1,3-Dihydroxyacetone by glycerol dehydrogenase Co-Expressed with an NADH oxidase for cofactor regeneration, Biotechnol. Lett. 38 (9) (2016) 1559–1564, https://doi.org/10.1007/s10529-016-2130-3.

[11] V. Cracan, D.V. Titov, H. Shen, Z. Grabarek, V.K. Mootha, A genetically encoded tool for manipulation of NADP+/NADPH in living cells, Nat. Chem. Biol. 13 (10) (2017) 1088–1095, https://doi.org/10.1038/nchembio.2454.

[12] S.A. Ahmed, A. Claiborne, The streptococcal flavoprotein NADH oxidase, J. Biol. Chem. 264 (33) (1989) 19856–19863, https://doi.org/10.1016/S0021-9258(19)47189-5.

[13] Argyrou, A.; Blanchard, J. S. Flavoprotein disulfide reductases: Advances in Chemistry and Function..

[14] T.C. Mallett, D. Parsonage, A. Claiborne, Equilibrium analyses of the active-site asymmetry in enterococcal NADH oxidase: role of the cysteine-sulfenic acid redox center, Biochemistry 38 (10) (1999) 3000–3011, https://doi.org/10.1021/bi9817717.

[15] R. Kellner, R. Malempré, J. Vandenameele, A. Brans, A.-F. Hennen, N. Rochus, A. Di Paolo, M. Vandevenne, A. Matagne, Protein formulation through automated screening of pH and buffer conditions, using the robotein® high throughput facility, Eur. Biophys. J. 50 (3) (2021) 473–490, https://doi.org/10.1007/s00249-021-01510-y.

[16] E. Krissinel, K. Henrick, Inference of macromolecular assemblies from crystalline state, J. Mol. Biol. 372 (3) (2007) 774–797, https://doi.org/10.1016/j.jmb.2007.05.022.

[17] The PyMOL Molecular Graphics System, Version 2.0 Schrödinger, LLC.

[18] E. Jurrus, D. Engel, K. Star, K. Monson, J. Brandi, L.E. Felberg, D.H. Brookes, L. Wilson, J. Chen, K. Liles, M. Chun, P. Li, D.W. Gohara, T. Dolinsky, R. Konecny, D.R. Koes, J.E. Nielsen, T. Head-Gordon, W. Geng, R. Krasny, G. Wei, M.J. Holst, J.A. McCammon, N.A. Baker, Improvements to the APBS biomolecular solvation software suite, Protein Sci. 27 (1) (2018) 112–128, https://doi.org/10.1002/pro.3280.

[19] S.F. Altschul, W. Gish, W. Miller, E.W. Myers, D.J. Lipman, Basic local alignment search tool, J. Mol. Biol. 215 (3) (1990) 403–410, https://doi.org/10.1016/S0022-2836(05)80360-2.

[20] F. Madeira, M. Pearce, A.R.N. Tivey, P. Basutkar, J. Lee, O. Edbali, N. Madhusoodanan, A. Kolesnikov, R. Lopez, Search and sequence analysis tools services from EMBL-EBI in 2022, Nucleic Acids Res. 50 (W1) (2022) W276–W279, https://doi.org/10.1093/nar/gkac240.

[21] K. Schwinn, N. Ferré, M. Huix-Rotllant, UV-Visible absorption spectrum of FAD and its reduced forms embedded in a cryptochrome protein, Phys. Chem. Chem. Phys. 22 (22) (2020) 12447–12455, https://doi.org/10.1039/D0CP01714K.

[22] P. Müller, J.-P. Bouly, K. Hitomi, V. Balland, E.D. Getzoff, T. Ritz, K. Brettel, ATP binding turns plant cryptochrome into an efficient natural photoswitch, Sci. Rep. 4 (1) (2014) 5175, https://doi.org/10.1038/srep05175.

[23] E.J. Faeder, L.M. Siegel, A rapid micromethod for determination of FMN and FAD in mixtures, Anal. Biochem. 53 (1) (1973) 332–336, https://doi.org/10.1016/0003-2697(73)90442-9.

[24] M.S. Pereira, S.S. De Araújo, R.A.P. Nagem, J.P. Richard, T.A.S. Brandão, The role of remote flavin adenine dinucleotide pieces in the oxidative decarboxylation catalyzed by salicylate hydroxylase, Bioorg. Chem. 119 (2022) 105561, https://doi.org/10.1016/j.bioorg.2021.105561.

[25] J.C. Encarnação, P. Barta, T. Fornstedt, K. Andersson, Impact of assay temperature on antibody binding characteristics in living cells: a case study, Biomed. Rep 7 (5) (2017) 400–406, https://doi.org/10.3892/br.2017.982.

[26] M. Yan, W. Yin, X. Fang, J. Guo, H. Shi, Characteristics of a water-forming NADH oxidase from *Methanobrevibacter smithii* , an archaeon in the human gut, Biosci. Rep. 36 (6) (2016) e00410, https://doi.org/10.1042/BSR20160357.

[27] F.-L. Li, Y. Shi, J.-X. Zhang, J. Gao, Y.-W. Zhang, Cloning, expression, characterization and homology modeling of a novel water-forming NADH oxidase from Streptococcus mutans ATCC 25175, Int. J. Biol. Macromol. 113 (2018) 1073–1079, https://doi.org/10.1016/j.ijbiomac.2018.03.016.

[28] S.M. McClure, P.L. Ahl, J.T. Blue, High throughput differential scanning fluorimetry (DSF) formulation screening with complementary dyes to assess protein unfolding and aggregation in presence of surfactants, Pharm. Res. 35 (4) (2018) 81, https://doi.org/10.1007/s11095-018-2361-1.

[29] G. Žoldák, R. Šuťák, M. Antalík, M. Sprinzl, E. Sedlák, Role of conformational flexibility for enzymatic activity in NADH oxidase from *thermus thermophilus*: flexibility of the NADH oxidase active site, Eur. J. Biochem. 270 (24) (2003) 4887–4897, https://doi.org/10.1046/j.1432-1033.2003.03889.x.

[30] G.T. Lountos, R. Jiang, W.B. Wellborn, T.L. Thaler, A.S. Bommarius, A.M. Orville, The crystal structure of NAD(P)H oxidase from lactobacillus sanfranciscensis: insights into the conversion of O2 into two water molecules by the flavoenzyme, Biochemistry 45 (32) (2006) 9648–9659, https://doi.org/10.1021/bi060692p.

[31] C. Nowak, B. Beer, A. Pick, T. Roth, P. Lommes, V. Sieber, A water-forming NADH oxidase from Lactobacillus pentosus suitable for the regeneration of synthetic biomimetic cofactors, Front. Microbiol. 6 (2015), https://doi.org/10.3389/fmicb.2015.00957.

[32] Y.-W. Zhang, M.K. Tiwari, H. Gao, S.S. Dhiman, M. Jeya, J.-K. Lee, Cloning and characterization of a thermostable H2O-Forming NADH oxidase from Lactobacillus rhamnosus, Enzym. Microb. Technol. 50 (4–5) (2012) 255–262, https://doi.org/10.1016/j.enzmictec.2012.01.009.

[33] J.-D. Zhang, Z.-M. Cui, X.-J. Fan, H.-L. Wu, H.-H. Chang, Cloning and characterization of two distinct water-forming NADH oxidases from Lactobacillus pentosus for the regeneration of NAD, Bioproc. Biosyst. Eng. 39 (4) (2016) 603–611, https://doi.org/10.1007/s00449-016-1542-8.

[34] G. Žoldák, A. Musatov, M. Stupák, M. Sprinzl, E. Sedlák, pH-Induced changes in activity and conformation of NADH oxidase from Thermus thermophilus, Gen. Physiol. Biophys. 24 (3) (2005) 279–298, https://doi.org/10.1002/pro.2693.